JOURNAL OF CATALYSIS **167,** 66–76 (1997)
ARTICLE NO. CA971546

Working Mechanism of Oxide Catalysts in the Partial Oxidation of Methane to Formaldehyde

II. Redox Properties and Reactivity of SiO_2, MoO_3/SiO_2, V_2O_5/SiO_2, TiO_2, and V_2O_5/TiO_2 Systems

Francesco Arena,* Nicola Giordano,†,‡ and Adolfo Parmaliana*,‡

*Dipartimento di Chimica Industriale, Università degli Studi di Messina, Salita Sperone c.p. 29, I-98166 S. Agata, Messina, Italy; and ‡Istituto CNR-TAE, Salita S. Lucia 39, I-98126 S. Lucia, Messina, Italy

Received February 27, 1996; revised November 12, 1996

The redox behaviour and the oxygen chemisorption of SiO_2, MoO_3/SiO_2, V_2O_5/SiO_2, TiO_2, and V_2O_5/TiO_2 systems have been systematically evaluated by H_2 and CH_4 temperature programmed reduction (i.e., H_2-TPR, CH_4-TPR) and high temperature oxygen chemisorption (HTOC) measurements, respectively. The influence of the oxide loading on the *surface structure* and *dispersity* of MoO_3/SiO_2 and V_2O_5/SiO_2 catalysts has been assessed. CH_4-TPR measurements indicate that the activity–selectivity pattern of oxide catalysts in MPO (A. Parmaliana and F. Arena, 1997, *J. Catal.* 166, 000–000) is controlled by their capability to interact with CH_4 undergoing a redox cycle under reaction conditions. The opposite effect of MoO_3 and V_2O_5 promoters on the catalytic functionality of the "precipitated" silica support has been explained in terms of a different reducibility of MoO_3 and V_2O_5 "surface species." The nature of the support as well as the level of the oxide loading affect the "reactivity" of lattice oxygen of supported systems determining their catalytic behaviour in MPO. The most effective reaction mechanism leading to the primary formation of HCHO implies the direct participation of gas-phase oxygen, while the involvement of bulk-lattice oxygen ions in the process of product formation mainly leads to CO_x. The interaction occurring between catalyst surface and reaction mixture under steady-state conditions is addressed.

INTRODUCTION

One of the most controversial issues of the catalytic partial oxidation of hydrocarbons on oxide systems remains the role of the catalyst lattice oxygen ions. Although it is ascertained that most partial oxidation reactions proceed according to the Mars–van Krevelen-type (or redox) mechanism, implying the occurrence of a reduction/oxidation cycle on the catalyst surface via "lattice oxygen ions" (2), the "working mechanism" (3–15) as well as the nature of the active centres of MPO catalysts (5–10, 16) are still topics of debate. The assessment of the reaction pathways of MPO over oxide catalysts is rather complicated since the high reaction temperatures (500–700°C) enable uncontrolled side reactions between gas-phase reactants and catalytic surface. Advanced isotopic labeling (11, 12, 15) and transient techniques (6–8, 11, 12) have been used to probe the origin of the oxygen species incorporated into reaction products. However, the capability of oxygenated compounds (i.e., HCHO, CO, CO_2) to easily undergo isotopic exchange with the catalyst oxygen ions (11, 12) has impeded the ascertainment of the contribution of surface or lattice oxygen species in the activation of methane and/or product formation (7, 8, 10, 11, 15). On this account, comparing the reaction rate in the presence and absence of gas-phase O_2, we previously argued that the MPO on silica based oxide catalysts, in the range 550–650°C, mainly proceeds via a *concerted mechanism* involving the activation of gas-phase oxygen on the "reduced sites" of the catalyst surface (7, 8). Moreover, it has been documented that the reaction pathways of MPO could depend on the nature of the catalyst (i.e., bulk or supported oxide), type of support (11, 17), and reaction temperature (7, 8, 17).

As the superior performance of MoO_3 and V_2O_5 as promoters of the activity of the SiO_2 support in the MPO, several studies have been aimed at defining the surface features of V_2O_5/SiO_2 (5, 11, 18, 19) and MoO_3/SiO_2 (12, 13, 19) systems attempting also to relate the reactivity with reducibility pattern and surface properties. A positive effect of the oxide dispersion (i.e., monolayer distribution) on the activity–selectivity pattern of both MoO_3/SiO_2 (13–15) and V_2O_5/SiO_2 (5, 18, 19) catalysts has been generally recognized. Nevertheless, since no great attention has been paid to evaluating the interactions between oxide catalyst and reaction mixture (i.e., CH_4 and O_2) under steady-state conditions (17) and considering the limitations connected with the traditional "single point" evaluation of the activity of MPO catalysts, ambiguous conclusions about the influence of promoters on the reactivity of the SiO_2 support (3–10,

†Deceased.

0021-9517/97 $25.00

19–23) as well as about the surface pathways of the title reaction (6–15, 20) were drawn.

Therefore, this paper is aimed at relating thoroughly the catalytic pattern of oxide catalysts, previously probed by temperature programmed reaction tests (1), with their physico-chemical properties evaluated by H_2- and CH_4-temperature programmed reduction and high temperature oxygen chemisorption measurements. Basic insights into the role of "lattice oxygen ions" and "working mechanism" of oxide catalysts in the title reaction are also provided.

EXPERIMENTAL

Catalysts

Differently loaded MoO_3/SiO_2, V_2O_5/SiO_2, and V_2O_5/TiO_2 catalysts were prepared according to the procedure described in detail elsewhere (1) using commercial "precipitated" silica, PS (Si 4-5P Grade, Akzo product; BET surface area, 400 $m^2\,g^{-1}$), and TiO_2 (GVA-500, Corning Glass product, BET surface area, 45 $m^2\,g^{-1}$) samples as support.

Commercial MoO_3 and V_2O_5 (Aldrich, analytical grade) samples were also used.

Before any characterization test, all the catalyst samples were pretreated *in situ* at 600°C for 1 h under a 15% O_2/He flow.

Catalyst Characterization

H_2-temperature programmed reduction (H_2-TPR) measurements were performed in a conventional apparatus operating in both pulse and continuos flow modes (1) using a linear quartz gradientless microreactor (i.d., 4 mm; length, 200 mm) and a 6% H_2/Ar mixture flowing at 60 STP $cm^3\,min^{-1}$. The reducing mixture was purified by passing it through a bed of activated molecular sieves and then over an Oxysorb adsorbent (Alltech product) kept at room temperature to remove any water and oxygen, respectively. All the experiments were carried out in the range 200–1200°C with a heating rate of 20°C min^{-1}. The H_2 consumption was monitored by a thermoconductivity detector (TCD) connected to a personal computer for data storage and processing. The sample weight was set between 0.002 and 0.25 g so to have a total H_2 consumption lower than 50 μmol in order to avoid mass and heat transfer limitations. The TCD response was quantitatively calibrated, proving linear in the whole investigated range of temperatures, by monitoring the reduction of known amounts of Cu^{II}, Ni^{II}, and Sn^{IV} oxides. Under such experimental conditions, TPR proved to be very reliable and accurate both in peak position (±5°C) and hydrogen consumption (±5%).

CH_4-temperature programmed reduction (CH_4-TPR) measurements were performed in the above flow apparatus using a linear quartz microreactor (i.d., 6 mm; length, 200 mm) connected on line with the QMS operating in the previously described conditions (1). CH_4-TPR tests were run in the range 400–800°C with β equal to 10°C min^{-1}, by using a 10% CH_4/He reduction mixture flowing at 50 STP $cm^3\,min^{-1}$ on 0.15–0.40 g of catalyst. CH_4-TPR mass spectra were obtained according to the procedure described in Ref. (1). The formulae [2] and [3] were used for the calculation of the reaction rate and rate of product formation (1), the rate of lattice oxygen consumption being obtained from the sum of oxygen atoms inserted into product molecules (i.e., HCHO; CO, CO_2, and H_2O).

High temperature oxygen chemisorption (HTOC) measurements of MoO_3/SiO_2 and V_2O_5/SiO_2 catalysts were performed in the above apparatus in a pulse mode using He as carrier gas (30 STP $cm^3\,min^{-1}$), according to the procedures elsewhere described (24, 25). Before measurements MPS and VPS catalyst samples (0.03–0.12 g) were reduced in a H_2 flow (25 STP $cm^3\,min^{-1}$) for 2 h at 357 and 367°C, respectively, and then flushed at the same temperature for 30 min in He carrier flow. Then, O_2 pulses (V_{pulse}, 4.3 μmol) were injected onto the carrier gas until saturation of the sample was attained. The O_2 uptake was quantified by a TCD connected to a DP 700 data processor (Carlo Erba Instruments). Under such conditions the reproducibility of O_2 uptake data was better than ±5%.

RESULTS

H_2-Temperature Programmed Reduction (H_2-TPR)

H_2-TPR of MoO_3/SiO_2 (MPS) catalysts. The H_2-TPR profiles of PS, differently loaded MPS catalysts, and bulk MoO_3 in the range 200–1200°C are comparatively shown in Fig. 1, while the onset temperature of reduction ($T_{o,red}$), the temperature of peak maxima (T_{Mi}), and the H_2 consumption values, calculated from the integral of the H_2-TPR curve up to 1200°C, are summarised in Table 1.

The H_2-TPR pattern of the bare PS carrier (Fig. 1a) does not show any hydrogen consumption up to ca. 900°C; thereafter, a very slight and featureless baseline drift signals an incipient reactivity of the system towards H_2 (Table 1).

A wide and convoluted band of H_2 consumption starting ($T_{o,red}$) at T ranging between 435 (MPS 7) and 486°C (MPS 2) and spanning a T range of 700–800°C accounts for

TABLE 1

H_2-TPR of Differently Loaded MPS Catalysts and Bulk MoO_3

Catalyst	$T_{o,red}$ (°C)	T_{M1} (°C)	T_{M2} (°C)	T_{M3} (°C)	T_{M4} (°C)	H_2 consumption (μmol g_{cat}^{-1})	R ($mol_{H_2}\,mol_{MoO_3}^{-1}$)
PS	908	—	—	—	—	13	—
MPS 2	486	—	—	—	917	410	2.95
MPS 4	436	588	765	—	—	827	2.98
MPS 7	435	574	703	—	—	1,470	3.02
MoO_3	532	—	763	840	—	20,900	3.01

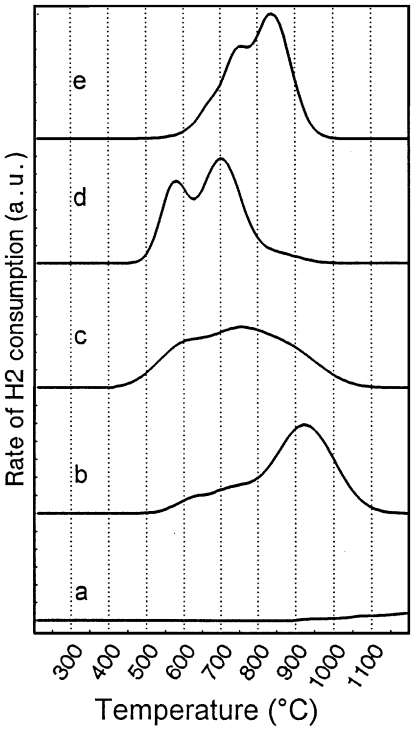

FIG. 1. H_2-TPR profiles of (a) PS, (b) MPS 2, (c) MPS 4, (d) MPS 7, and (e) bulk MoO_3.

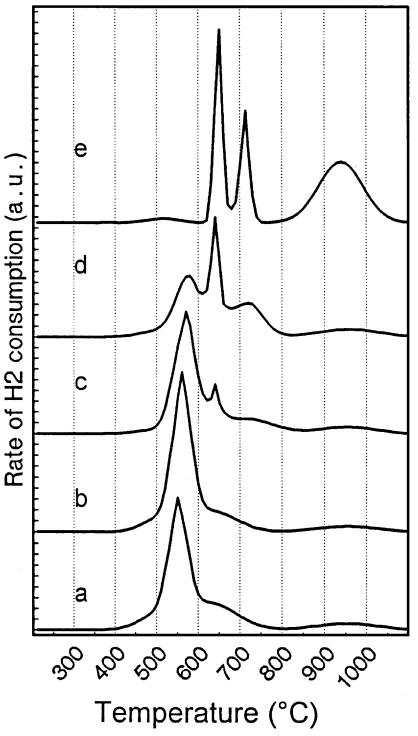

FIG. 2. H_2-TPR profiles of (a) VPS 2, (b) VPS 4, (c) VPS 10, (d) VPS 20, and (e) bulk V_2O_5.

the stoichiometric reduction of MoO_3 to Mo^0 in all MPS catalysts (Table 1). The spectrum of the low loaded MPS 2 catalyst features a low rate of H_2 consumption up to ca. 800°C; thereafter the reduction rate increases sharply giving rise to a main reduction peak with maximum at 934°C (Fig. 1b). The increase in the MoO_3 loading from 2 to 4 wt% (MPS 4) causes a marked shift of $T_{o,red}$ to lower T (436°C) and a concomitant enhancement of the reduction kinetics at lower T (<800°C), giving rise to a convoluted reduction profile with two unresolved peaks with maxima at 588 and 765°C, respectively (Fig. 1c). A further increase in the MoO_3 loading strongly enhances the reduction rate of the system at $T < 800$°C (Fig. 1d), even if the $T_{o,red}$ value (435°C) of the MPS 7 catalyst keeps equal to that of the MPS 4 sample (436°C). The reduction pattern consists of two sharp peaks with resolved maxima at 574 and 703°C, respectively, along with a shoulder of H_2 consumption in the range 800–1050°C.

The reduction of the bulk MoO_3 (Fig. 1e) starts at T considerably higher ($T_{o,red} = 532$°C) than those found for supported MPS systems (Table 1), resulting in two overlapped peaks with maxima at 763 and 840°C (Table 1) likely accounting for the step-wise ($Mo^{VI} \rightarrow Mo^{IV} \rightarrow Mo^0$) reduction of MoO_3 to Mo^0.

H_2-TPR of V_2O_5/SiO_2 (VPS) catalysts. The H_2-TPR profiles of differently loaded VPS catalysts and bulk V_2O_5 in the range 200–1100°C are shown in Fig. 2. The onset temperature of reduction ($T_{o,red}$), the temperature of peak maxima (T_{Mi}), and the values of the integral H_2 consumption, accounting for the stoichiometric reduction of V^{5+} to V^{3+} in both VPS and bulk V_2O_5 systems, are summarized in Table 2.

The H_2-TPR pattern of the low VPS 2 catalyst (Fig. 2a) entails a very sharp reduction peak with the maximum (T_{M1}) at 551°C, slightly asymmetric on the high temperature side due to the presence of a shoulder of H_2 consumption zeroing at $T \approx 850$°C. The $T_{o,red}$ is equal to 360°C, being the lowest found in the series (Table 2). An increase in the V_2O_5 loading to 5 wt% (VPS 5) does not substantially affect the reduction pattern of the system either in terms of $T_{o,red}$ (364°C) or in peak shape (Fig. 2b) even if the T_{M1} is slightly displaced to higher T (561°C). More evident changes in

TABLE 2

H_2-TPR of Differently Loaded VPS Catalysts and Bulk V_2O_5

Catalyst	$T_{o,red}$ (°C)	T_{M1} (°C)	T_{M2} (°C)	T_{M3} (°C)	T_{M4} (°C)	H_2 consumption (μmol g_{cat}^{-1})	R (mol_{H_2} $mol_{V_2O_5}^{-1}$)
PS	908	—	—	—	—	13	—
VPS 2	360	551	—	—	—	211	1.92
VPS 5	364	561	—	—	962	575	1.98
VPS 10	372	571	638	730	960	1,132	2.04
VPS 20	397	584	645	722	961	2,215	1.94
V_2O_5	434	519	649	716	939	11,000	2.00

the reduction pattern of the V_2O_5/SiO_2 system (Fig. 2c) occur at higher V_2O_5 loading (VPS 10), since the $T_{o,red}$ value further shifts to higher T (372°C) while a broadening of T_{M1} peak along with a further rise of T_{M1} value (571°C) are recorded. Moreover, two new smaller peaks, bearing resolved maxima at 638 (T_{M2}) and 730°C (T_{M3}), are observable (Fig. 2d). At a loading level of 20 wt% (VPS 20), the T_{M1} peak decreases considerably in intensity assuming an asymmetric shape, while its maximum further shifts to higher T ($T_{M1} = 584$°C); T_{M2} and T_{M3} peaks rise in intensity, the former becoming the predominant one; however, no significant changes in their maxima values with respect to VPS 10 system (Table 2) are detected.

The H_2-TPR pattern of the bulk V_2O_5 (Fig. 2e) displays two very sharp, partially overlapping, reduction peaks centered at 649°C (T_{M2}) and 716°C (T_{M3}), respectively, and a third broader peak at higher T with maximum at 939°C (T_{M4}). The relative intensity of such three peaks accounts for the following sequential reduction path: $V_2O_5 \rightarrow V_6O_{13} \rightarrow VO_2 \rightarrow V_2O_3$.

H_2-TPR of TiO_2 and 2 wt% V_2O_5/TiO_2 (VT 2) catalysts. The H_2-TPR spectra of TiO_2 carrier and VT 2 catalyst in the range 200–1000°C are shown in Fig. 3, while the onset temperature of reduction ($T_{o,red}$), the temperature of peak maxima (T_{Mi}), and the H_2 consumption values are compared with those of PS carrier and VPS 2 counterpart systems in Table 3. Differently from PS support (Fig. 1a), TiO_2 sample outlines a significant reactivity towards H_2 also at low T. The related reduction profile (Fig. 3a) shows a broad reduction peak ($T_{o,red} = 430$°C) with maximum at 574°C along with an incipient H_2 consumption at $T > 630$°C. The amount of H_2 consumption up to 1000°C (304 μmol g^{-1}) corresponds to an average substoichiometric reduction of Ti^{4+} to $Ti^{3.95+}$ (Table 3).

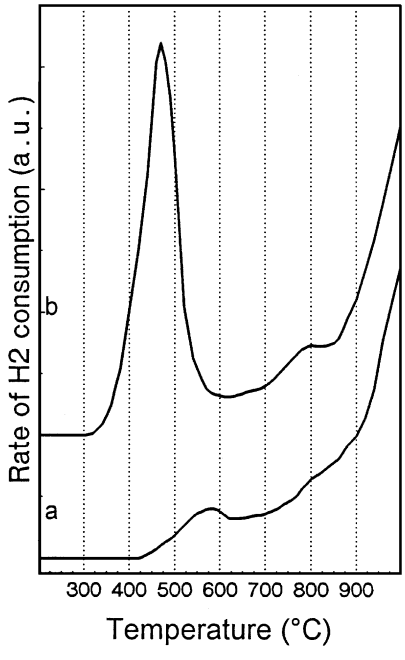

FIG. 3. H_2-TPR profiles of (a) TiO_2 and (b) VT 2 samples.

TABLE 3

H_2-TPR of TiO_2 and VT 2 Catalyst

Catalyst	$T_{o,red}$ (°C)	T_{M1} (°C)	T_{M2} (°C)	T_{M3} (°C)	T_{M4} (°C)	H_2 consumption (μmol g_{cat}^{-1})
TiO_2	430	574	—	—	—	304
VT 2	315	468	—	—	794	533
PS	908	—	—	—	—	13
VPS 2	360	551	—	—	966	211

The reduction pattern of VT 2 catalyst (Fig. 3), compared to the same loaded VPS 2 system (Fig. 2b), provides evidence of a promoting effect of the TiO_2 support on the reduction of V_2O_5, as pointed out by the marked shift of both $T_{o,red}$ (315°C) and T_{M1} (468°C) to lower T (Table 3). At $T > 600$°C the rate of H_2 consumption rises monotonically with T according to the trend already found for the bare TiO_2 support (Fig. 3). The overall H_2 consumption (533 μmol g^{-1}) accounts for the stoichiometric reduction of V_2O_5 to V_2O_3 (220 μmol g^{-1}) and the aforesaid incipient reduction of TiO_2 support (313 μmol g^{-1}).

High Temperature Oxygen Chemisorption (HTOC) of MPS and VPS Catalysts

The values of HTOC uptake oxide dispersion (O/Me) for MPS and VPS catalysts heat treated at 600°C are summarised in Table 4.

The O_2 chemisorption of the bare SiO_2 sample is very low (0.5 μmol g^{-1}), being more than one order of magnitude lower than those of promoted catalysts.

The O_2 uptakes of MPS catalysts increase with the loading from 6.1 (MPS 2) to 111.5 μmol g^{-1} (MPS 7). The oxide dispersion (O/Mo) results very low for the MPS 2 catalyst (8.8%), while it suddenly increases for MPS 4 sample

TABLE 4

HTOC Characterization Data of MPS and VPS Catalysts

Catalyst	O_2 uptake (μmol g_{cat}^{-1})	O/Me (%)
PS	0.5	—
MPS 2	6.1	8.8
MPS 4	66.4	47.8
MPS 7	111.5	45.9
VPS 2	68.0	61.9
VPS 5	186.9	64.5
VPS 10	262.1	46.6
VPS 20	328.3	28.7

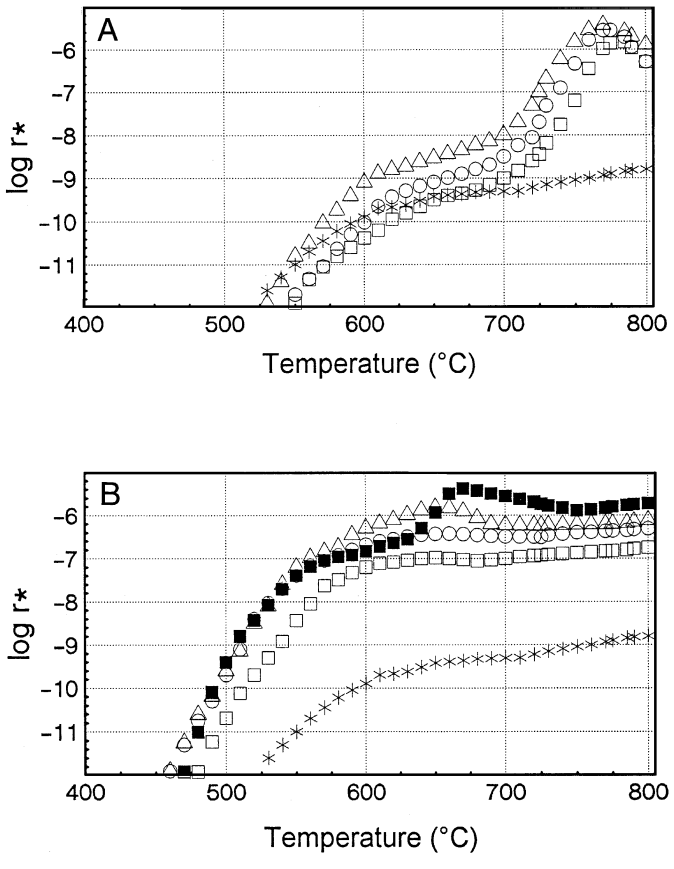

FIG. 4. CH_4-TPR. Rate of lattice oxygen consumption, r^*, vs T of (A) MPS (⊛), PS; □, MPS 2; ○, MPS 4; △, MPS 7) and (B) VPS (∗, PS; □, VPS 2; ○, VPS 5; △, VPS 10; ■, VPS 20) catalysts.

(47.8%), keeping unchanged (45.9%) at higher MoO_3 loading (MPS 7).

The oxygen uptake of VPS catalysts increases monotonically with the loading attaining the maximum value ($\approx$328 μmol g^{-1}) for the VPS 20 sample. The oxide dispersion reaches the maximum value (60–62%) for low–medium loaded (2–5 wt%) catalysts; thereafter at loadings higher than 5% it decreases to 46.6 and 28.7% for VPS 10 and VPS 20 samples, respectively.

CH_4-Temperature Programmed Reduction (CH_4-TPR)

CH_4-TPR of MPS and VPS catalysts. Basic information on the reactivity of lattice oxygen ions of both MPS and VPS catalysts towards CH_4 has been achieved by performing a series of temperature programmed reduction measurements in the range 400–800°C using CH_4 as reactant (CH_4-TPR).

The rate of lattice oxygen consumption (r^*, $mol_O\ s^{-1}\ g^{-1}$) as a function of temperature for differently loaded MPS (A) and VPS catalysts (B) is shown in Fig. 4, while the rate of CH_4 conversion and the product distribution in the presence (r_0) and absence of gas-phase oxyen (r_1) at various T for PS, MPS 4, and VPS 5 catalysts are compared in Table 5 (The data relative to MPS 2, MPS 7, and VPS 2, VPS 10, and VPS 20 samples have been omitted because of a substantial analogy with those of the homologous MPS 4 and VPS 5 catalysts, respectively). In particular, these data can be rationalized as follows:

(i) The bare PS support exhibits a very low reactivity towards CH_4, resulting more than three orders of magnitude lower than r_0 in the whole range 550–800°C (Table 5). The only products observed in the absence of gas-phase oxygen are HCHO and C_2. Formaldehyde is the main product of the interaction of CH_4 with PS surface in the range 550–725°C (Table 5); thereafter a prevailing contribution of C_2 products, paralleled by a rise in the H_2 concentration, is observed. The value of r^* rises slightly in the range 600–800°C, reaching a maximum value of $\approx 2 \times 10^{-9}$ mol $s^{-1}\ g_{cat}^{-1}$ at 800°C (Fig. 4).

(ii) MPS catalysts at $T < 650$°C present a very low reactivity towards CH_4 comparable with that of the bare PS support (Table 5). At higher T, the values of r^* become much higher than the corresponding values of PS (Fig. 4A) and then a substantial increase in the rate of formation of oxygenated products (e.g., HCHO, CO, and CO_2) is observed (Table 5). The r_0 values in the range 550–700°C are two to three orders of magnitude lower than r_1 ones, whereas at $T > 700$°C such difference becomes considerably smaller (Table 5). At $T > 700$°C, a significant carbon deposition on the surface of MPS catalysts has been noticed.

(iii) All VPS catalysts exhibit a high reactivity to CH_4 and consequently high values of r^* already at T lower than 500°C (Fig. 4B). The reaction products are HCHO, CO, CO_2, and C_2 (Table 5). HCHO is the primary product of reaction of CH_4 with the lattice oxygen of VPS catalysts. At $T > 500$°C a sudden drop in the rate of HCHO formation occurs and minor amounts of CO_2 are detected. At $T > 650$°C, CO and C_2 become the main reaction products (Table 5), while a decrease of r^* is observed (Fig. 4B). A maximum r^* at $T \approx 650$°C appears in the CH_4-TPR spectrum of the VPS 10 sample which becomes considerably more pronounced on the VPS 20 system (Fig. 4B). Also for VPS systems the values of r_0 in the range 450–725°C result one to two orders of magnitude lower than those of r_1 (Table 5).

CH_4-TPR of TiO_2 and VT 2 catalysts. The trend of the rate of lattice oxygen consumption (r^*) in the range 400–800°C for TiO_2 and VT 2 (2% V_2O_5/TiO_2) catalysts are compared with those of PS and VPS 2 (2% V_2O_5/SiO_2) catalyst in Fig. 5, while the values of CH_4 conversion and product selectivity in the presence (r_0) and absence of gas-phase oxygen (r_1) at various T are listed in Table 6. In the absence of oxygen, titania reacts with CH_4 at lower T (430°C) with respect to PS sample attaining r^* values one order of magnitude higher than those of the latter system in the whole range 400–800°C (Fig. 5). CO is the main product

TABLE 5

Methane Partial Oxidation on PS, MPS 4, and VPS 5 Catalysts

Catalyst	T_R (°C)	r_0[a] (μmol s^{-1} g^{-1})	Selectivity (%) HCHO	CO	CO_2	C_2	r_1[b] (μmol s^{-1} g^{-1})	Selectivity[a] (%) HCHO	CO	CO_2	C_2
PS	550	5.0×10^{-6}	100	0	0	0	0.3	84	16	0	0
	650	1.2×10^{-4}	100	0	0	0	3.1	47	49	4	0
	725	7.3×10^{-4}	82	0	0	18	12.5	35	55	8	2
	750	5.0×10^{-4}	15	8	0	85	18.3	25	62	9	4
	800	1.3×10^{-3}	2	0	0	98	34.2	11	71	10	8
MPS 4	550	3.0×10^{-6}	100	0	0	0	0.1	96	4	0	0
	650	5.0×10^{-4}	90	10	0	0	1.2	50	35	15	0
	725	0.3	2	78	10	10	6.3	37	45	18	0
	750	1.2	1	76	11	12	10.8	33	48	18	1
	800	1.8	2	66	4	28	28.4	19	59	18	4
VPS 5	500	8.1×10^{-5}	35	65	0	0	0.2	78	22	0	0
	550	1.4×10^{-2}	15	85	0	0	1.2	46	51	3	0
	600	6.7×10^{-2}	10	90	0	0	4.6	29	64	7	0
	650	0.2	2	74	14	10	13.9	15	74	11	0
	700	2.7	0	68	16	17	34.3	6	81	14	0

Note. Rate of CH_4 conversion (r_0, r_1) and product selectivity in the absence (r_0) and presence (r_1) of gas-phase oxygen

[a] Values calculated from CH_4-TPR tests.

[b] Data taken from Ref. (1).

of the interaction between CH_4 and TiO_2 surface at any T (Table 6), while smaller amounts of C_2 products are detected only at $T > 700$°C (Table 6).

The VT 2 catalyst in the absence of oxygen starts to interact with CH_4 at 400°C, exhibiting r^* values higher than those of the corresponding VPS 2 sample in the range 400–600°C (Fig. 5). A maximum r^* value at 540°C is observable. At $T \geq 650$°C the r^* on VT 2 catalyst keeps constant, following a trend analogous to that of the bare TiO_2 support (Fig. 5). CO is the main product of the interaction of CH_4 with lattice oxygen ions of VT 2 catalyst, though in the range 500–650°C some HCHO along with smaller amounts of CO_2 have been detected, at $T \geq 650$°C the formation of trace amounts of C_2 products has been observed (Table 6).

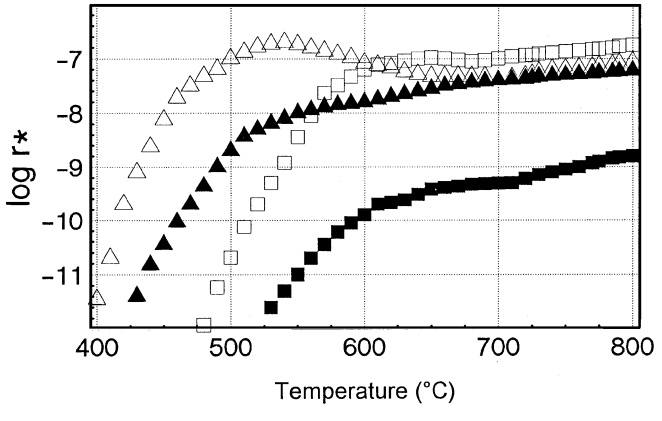

FIG. 5. CH_4-TPR. Rate of lattice oxygen consumption (r^*) vs T of (▲) TiO_2, (△) VT 2, (■) PS, and (□) VPS 2 catalysts.

Also for both TiO_2 and VT 2 catalysts the difference between r_0 and r_1 in the range 400–800°C is two to three orders of magnitude.

DISCUSSION

Influence of MoO_3 Loading on the Physico-Chemical and Catalytic Properties of MPS System

Previous TPR studies attempted to model the reduction pattern of MoO_3/SiO_2 catalysts according to the stepwise reduction process $Mo^{VI} \rightarrow Mo^{IV} \rightarrow Mo^0$ (26, 27). Various effects such as the different size and morphology of MoO_3 crystals, besides the presence of several noncrystalline MoO_3 forms, were invoked in order to explain the marked differences in the TPR patterns of MoO_3/SiO_2 catalysts with reference to the bulk MoO_3 system (26, 27). Comparative characterization studies of MoO_3 supported on different carriers (i.e., Al_2O_3, SiO_2, etc.) claimed a "weak-type" interaction between MoO_3 and SiO_2 in order to explain an easier reduction of MoO_3/SiO_2 catalysts (24, 26, 27). However, the wider band the H_2 consumption featuring the reduction pattern of MPS catalysts in comparison to bulk MoO_3 (Fig. 1) is diagnostic of a strong metal oxide–support interaction (13, 28) which markedly depresses the reduction of MoO_3 promoter. The marked differences in the TPR profiles of MPS catalysts (Fig. 1) as well as the random variations of the related reductin maxima (Table 1) do no allow an immediate rationalization of the reduction pattern of the MoO_3/SiO_2 system (Fig. 1). However, using a least-squares fitting program, such spectra have been resolved into the contribution of three discrete

TABLE 6

Methane Partial Oxidation on TiO_2 and VT 2 Catalysts

Catalyst	T_R (°C)	r_0[a] (μmol s^{-1} g^{-1})	Selectivity (%) HCHO	CO	CO_2	C_2	r_1[b] (μmol s^{-1} g^{-1})	Selectivity (%) HCHO	CO	CO_2	C_2
TiO_2	500	1.5×10^{-3}	0	100	0	0	0.3	0	100	0	0
	550	5.3×10^{-3}	0	100	0	0	0.5	3	96	1	0
	600	7.7×10^{-3}	0	100	0	0	1.2	5	92	3	0
	650	1.5×10^{-2}	0	100	0	0	3.8	5	88	7	0
	700	3.3×10^{-2}	0	97	0	3	9.5	5	85	9	1
	750	4.5×10^{-2}	0	86	0	14	19.3	4	80	14	2
	800	5.7×10^{-2}	0	79	0	21	25.5	3	76	19	2
VT 2	500	2.6×10^{-2}	35	65	0	0	0.2	0	96	4	0
	550	6.6×10^{-2}	15	85	0	0	0.9	2	91	7	0
	600	3.5×10^{-2}	10	90	0	0	2.9	3	83	14	0
	650	3.5×10^{-2}	2	74	14	10	9.7	2	76	22	0
	700	5.0×10^{-2}	0	68	16	16	24.7	1	64	35	0

Note. Rate of CH_4 conversion (r_0, r_1) and product selectivity in the absence (r_0) and presence (r_1) of gas-phase oxygen.
[a] Values calculated from CH_4-TPR tests.
[b] Data taken from Ref. (1).

Gaussian-shaped peaks (28). The deconvoluted TPR profiles of MPS 2, MPS 4, and MPS 7 samples are shown in Fig. 6, while the fitting parameters of TPR spectra, expressed as peak maximum position (M_i), full width at half maximum ($FWHM_i$), and percentage peak area (A_i, %) are reported in Table 7. It is assumed that the first two peaks (i.e., M_1 and M_2) monitor the step-wise reduction ($Mo^{VI} \rightarrow Mo^{IV} \rightarrow Mo^0$) of "$MoO_3$ crystallites" (*Mc*), while the third one (M_3) refers to the reduction ($Mo^{VI} \rightarrow Mo^0$) of "isolated molybdates" species (*Im*) (28). From a systematic inspection of the fitting parameters (Table 7), it arises that the intensity of the first two peaks, centered at 579–623°C (M_1) and 703–740°C (M_2), respectively, rises monotonically in intensity with MoO_3 loading; while the highest temperature peak (M_3), monitoring the reduction of *Im* species and lying in the range 855–928°C, decreases in intensity with the MoO_3 loading (28, 29). Notably, the shift on M_3 value towards lower *T*, occurring at higher MoO_3 loadings, reflects an improved reducibility of *Im* species, likely enabled by the "autocatalytic effect" exerted by the increased MoO_3 concentration (28).

On the whole, the surface composition of the differently loaded MPS catalysts, reported in Table 7 in terms of relative percentage and absolute concentration (μmol g^{-1}) of *Mc* and *Im* species, provides evidence of the influence of the loading on the surface structures of MoO_3/SiO_2 catalysts, allowing also the explaination of the unusual trend of the chemisorption data (Table 4). Indeed, the prevailing stabilization of "hardly reducible" *Im* species in MPS 2 sample (see Fig. 6 and Table 7) accounts for its small oxygen uptake and unusually low dispersion value (Table 4). At MoO_3 loadings higher than 2 wt%, the increasing formation of *Mc* (Table 7) enhances the reducibility of the system as well as the chemisorption capability and dispersion values (Table 4). Further insights into the surface structure and dispersion of differently loaded MPS catalysts are provided by the comparison of H_2-TPR spectra (Fig. 1) and FWHM of related fitting-peaks (Table 7). In fact, the

TABLE 7

Fitting Parameters of TPR Spectra and Concentration of *Mc* and *Im* Species in Differently Loaded MPS Catalysts

Catalyst	*Mc*[a] M_1 (°C)	$FWHM_1$ (°C)	A_1 (%)	M_2 (°C)	$FWHM_2$ (°C)	A_2 (%)	*Im* M_3 (°C)	$FWHM_3$ (°C)	A_3 (%)	Concentration % *Mc*	% *Im*	μmol·g^{-1} *Mc*	μmol·g^{-1} *Im*
MPS 2	623	105	7.6	736	139	15.1	928	179	77.3	22.7	77.3	31.5	107.4
MPS 4	585	129	22.1	730	182	44.9	878	185	33.0	67.0	33.0	186.1	91.7
MPS 7	579	95	30.8	703	125	62.1	855	172	7.1	92.9	7.1	451.6	34.5

[a] In order to satisfy the reduction stoichiometry of *Mc* according to the steps $Mo^{VI} \rightarrow Mo^{IV} \rightarrow Mo^0$, the ratio of the areas of the relative peaks was kept equal to 0.5 (±10%).

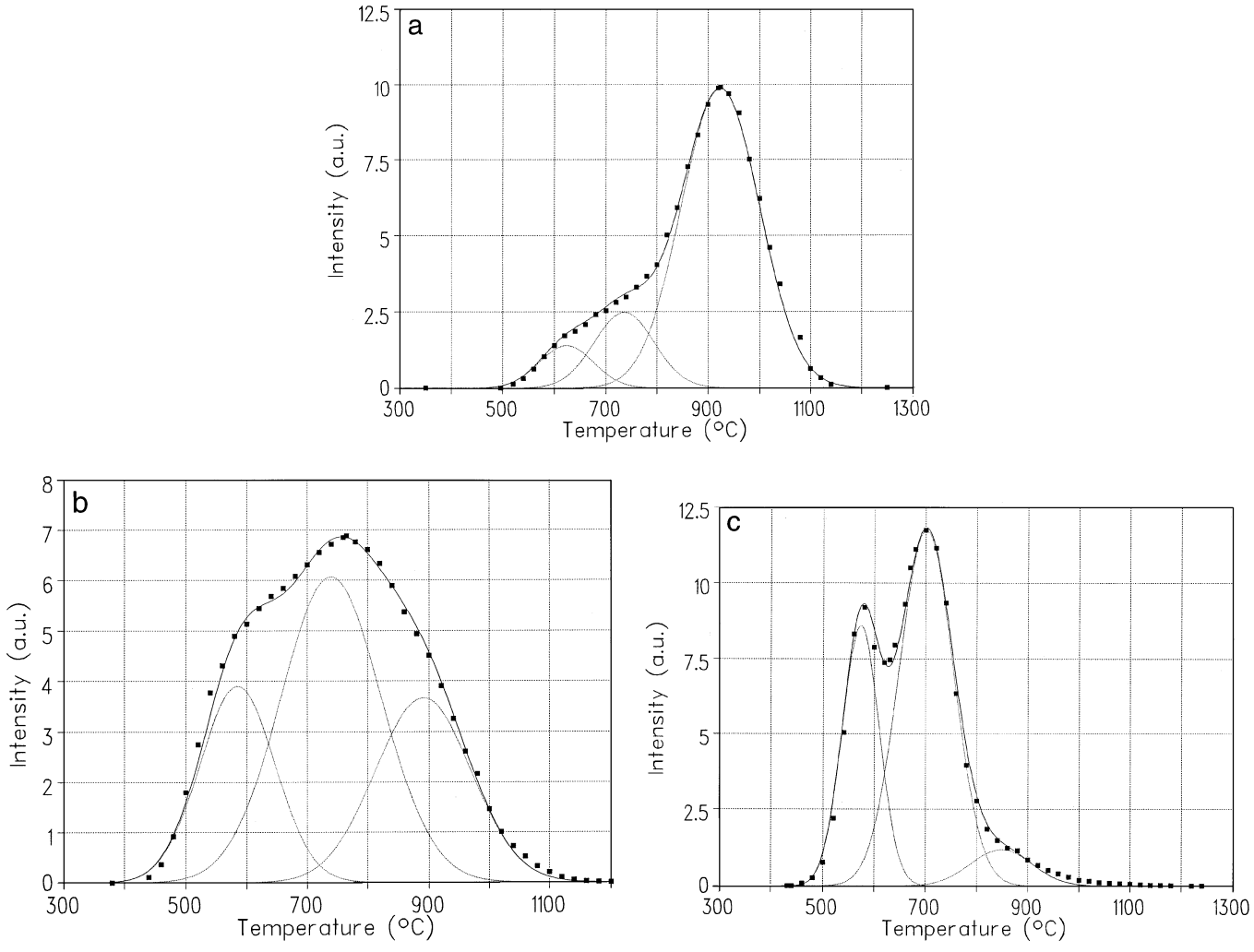

FIG. 6. Curve-fitted H_2-TPR spectra of differently loaded MPS catalysts : (a) MPS 2, (b) MPS 4, and (c) MPS 7.

remarkable broadness of M_1 and M_2 peaks of MPS 4 catalyst along with the absence of sharp features in the range 580–700°C, characteristic of the reduction of MoO_3 crystallites (Fig. 1c), likely indicate the presence of a "well dispersed" polymerized molybdenum oxide species, which should be the precursor of the *Mc* species rather than that of crystalline MoO_3 particles (28, 29). Therefore, also for the MPS 4 sample the dispersion degree calculated from HTOC data (Table 4) would be underestimated, being really much higher than that of MPS 7 catalyst (28).

On the basis of the above considerations, it can be inferred that three types of "surface sites" contribute to the reactivity of MoO_3/SiO_2 catalysts in MPO, namely; the *siloxane bridges* of the silica surface (30), the *Mo–O–Mo bridging functionalities*, and the *Mo=O terminal bonds* of *Mc* (12–14). Then, the catalytic pattern of MoO_3/SiO_2 system in MPO, at a given temperature, results in a complex function of density and activity of the various surface sites. On increasing the MoO_3 loading, the decrease in BET surface area (1) and the increasing coverage of the silica surface by the promoter concur to reduce the concentration of active sites of the SiO_2 surface, causing, mainly at $T \leq 650$°C, a progressive lowering in the SSA of MPS systems with respect to PS (1, 7, 8, 19, 22, 23). At higher T, the MoO_3 promoter, owing to its capability to interact with CH_4 molecules (Fig. 4A), improves the SSA of MPS catalysts with respect to PS (1). Then, the increasing oxygen uptake (Table 4), paralleling the higher concentration of *Mc* (Table 7), should account for the promoting effect of MoO_3 loading on both SSA and SP_{HCHO} of MPS catalysts at $T > 650$°C (1). This is well supported by the straight-line relationship between SP_{HCHO} at 700 and 800°C and HTOC uptake, shown in Fig. 7, which points to the specificity of "Mo=O" terminal bonds of MoO_3 crystallites towards HCHO formation (12–14, 31). Whereas the largest amount of "dispersed MoO_3 species" in MPS 4 catalyst signals the high tendency of "Mo–O–Mo" bridging sites in enabling total oxidation of either CH_4 or CO (1, 12–14).

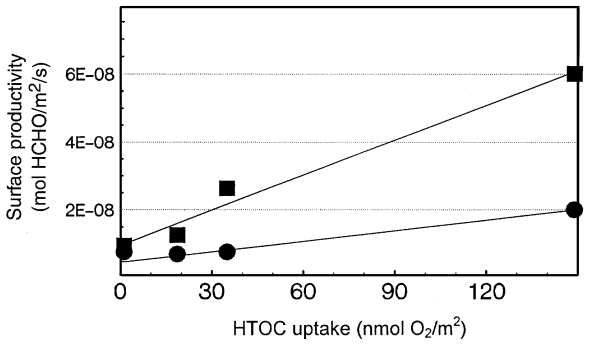

FIG. 7. Relationship between oxygen uptake and surface productivity of differently loaded MPS catalysts at 700°C (●) and 800°C (■).

Influence of V_2O_5 Loading on the Physico-Chemical and Catalytic Properties of VPS System

The very sharp reduction peak featuring the H_2-TPR spectra of low–medium (2–5.3 wt%) VPS catalysts is diagnostic of the presence of an *easily reducible* "surface V_2O_5 species." The highest dispersion of VPS 2 and VPS 5 systems (Table 4) allows the inference that on these systems V_2O_5 mainly exists in the form of well dispersed "isolated vanadyl species" (*Iv*), with V^{5+} in tetrahedral coordination (T_d) (25, 31, 32). However, the shoulder on the high *T* side of the main H_2-TPR peak (T_{M1}) indicates also the existence of minor amounts of less reducible polymeric vanadate species or V_2O_5 crystallites (33). At V_2O_5 loadings higher than 5 wt%, the concomitant shift of $T_{o,\,red}$ and T_{M1} to higher *T* (Table 2), the increasing intensity of T_{M2}–T_{M3} peaks, characteristic of the reduction of bulk V_2O_5 (Fig. 2), and the lowering in oxide dispersion (Table 4) altogether provide unambiguous evidence of the nucleation of VO_4^{3-} units into polymeric structures, like "polyvanadates" (*Pv*), and V_2O_5 clusters (*Vc*) with V^{5+} in square-pyramidal (S_p) and octahedral coordination (O_h), respectively (25, 32). In order to probe the validity of such statements, the dispersion values (O/V, %) of VPS samples are plotted against the relative intensity of T_{M1} peak (%) in Fig. 8. The straight-line relationship suggests that the oxygen chemisorption mostly occurs on coordinatively unsaturated (CUS) V^{III} sites formed by the reduction of isolated VO_4^{3-} species (25, 33). The decrease in oxide dispersion, occurring at loading higher than 5 wt%, parallels the increasing formation of "agglomerated" structures (i.e., *Pv* and *Vc*) entailing a lower percentage of CUS sites.

Considering the catalytic pattern of the VPS system, it can be inferred that the progressive loss in HCHO selectivity induced by the V_2O_5 loading (1), not counterbalanced by a corresponding increase in activity, mostly monitors a higher oxidation strength associated with the drop in V_2O_5 dispersion (5, 11, 18). This is supported by the fact that the oxygen species formed on the well dispersed T_d *Iv* yield the primary oxidation of CH_4 to HCHO (8, 11), whereas surface "V–O–V bridging sites" of bulk-like vanadia crystallites mainly enable secondary oxidation reactions leading to CO and CO_2 (11, 18, 32). On the other hand, the larger oxygen uptake of the highly loaded VPS 10 and VPS 20 Catalysts (Table 4), not corresponding to an increase in the SSA (1), probably points to a modification of the electronic properties of *Iv* induced by neighbouring *Pv* and *Vc* species.

Nature of the Reactivity of PS, MPS, and VPS Catalysts in the MPO

The H_2-TPR results indicate that a different metal oxide–support interaction enhances the reducibility of *Iv* and depresses that of *Im*, accounting for the opposite influence of V_2O_5 and MoO_3 promoters on the functionality of PS in MPO (7, 8, 19, 22, 23). However, the following findings still deserve scrutiny:

(i) the bare PS carrier exhibits SSA higher than that of MPS catalysts at $T \leq 650$°C (1), in spite of dramatic differences in both reducibility (Fig. 1) and chemisorption capability (Table 4);

(ii) the reducibility of MPS catalysts at $T < 800$°C increases with the oxide loading (Fig. 1), while the SSA at $T \leq 650$°C follows an opposite decreasing trend;

(iii) VPS catalysts exhibit remarkable differences in their catalytic behaviour, mainly in terms of HCHO selectivity, which cannot be fully explained on the basis of H_2-TPR and HTOC results;

(iv) although MPS and VPS catalysts present a considerable reduction rate at $T > 400$°C, these promoters differently affect the functionality of PS surface at $T \leq 650$°C (1).

As the H_2-TPR pattern is not adequate either to attain a full rationalization of the activity of the studied systems (1) or to explain the stabilisation of "reduced sites" under reaction conditions (7, 8), the interaction between catalyst surface and methane (CH_4-TPR) must be taken into

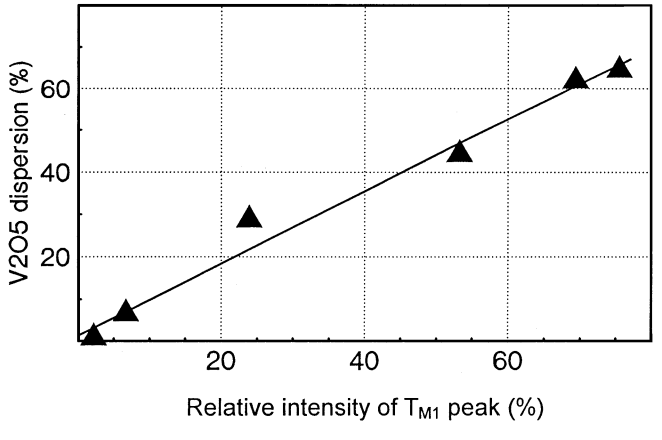

FIG. 8. Relationship between the oxide dispersion (O/V, %) and the relative intensity of T_{M1} TPR peak for differently loaded VPS catalysts.

account. Indeed, the slight rate of CH_4 conversion of the bare PS sample at $T \geq 550°C$ (Table 5) is indicative of the capability of silica surface to interact with CH_4 molecules (30, 34), unless the very low values of r^* rule out any activity of lattice oxygen ions. The product distribution of CH_4-TPR (Table 5) provides insights into the interaction paths between CH_4 and silica surface. In fact, the formation of HCHO at $T < 700°C$ likely signals the decomposition of the surface Si–O–CH_3 methoxy complex, while the prevailing formation of C_2 products at $T > 700°C$ is diagnostic of the gas-phase coupling of CH_3· methyl radicals likely arising from Si–CH_3 surface species (9). Besides, such a reactivity of the SiO_2 surface towards CH_4 accounts for the stabilization of reduced sites under reaction conditions which provide the formation of surface active oxygen species (e.g., O^-, O_2^-, O·, etc.) (7, 8).

For VPS catalysts a marked enhancement in the reactivity towards CH_4 (Table 5), due to the reduction of the promoter, is observed (Fig. 4B). The similar reactivity pattern of VPS catalysts at $T < 650°C$ reflects the easy reducibility of *Iv* species, while the sudden increase of r^* on VPS 20 sample at $T > 650°C$ (Fig. 4B) is attributable to the great mobility and availability of lattice oxygen ions in O_h *Vc* (32, 35–38). The highest performance of low–medium loaded (2–10 wt%) VPS catalysts in MPO thus stems from *Iv* species which have the capability of ensuring the formation of "active" oxygen species (32, 35) on the surface reduced sites (7, 8). The effectiveness of *Iv* species towards HCHO formation is proved by the exponential-like relationship between the specific oxide productivity at 600 and 650°C ($mol_{HCHO}\ g^{-1}_{V_2O_5}\ s^{-1}$) and V_2O_5 dispersion shown in Fig. 9. Therefore, the above evidences suggest that the highest value of E_{app} (47 kcal mol^{-1}) of VPS 20 catalyst features mainly the catalytic activity of *Pv* and *Vc* enabling CH_4 activation only at $T > 600°C$ (Fig. 4B). In fact, at higher V_2O_5 loadings (VPS 20), the extensive formation of V_2O_5 crystallites implies a change in the reaction mechanism (38) owing to the fast *incorporation* of "surface activated oxygen species" into lattice oxygen ions ($O^=$) which are less effective towards CH_4 activation but able to promote the consecutive oxidation of HCHO.

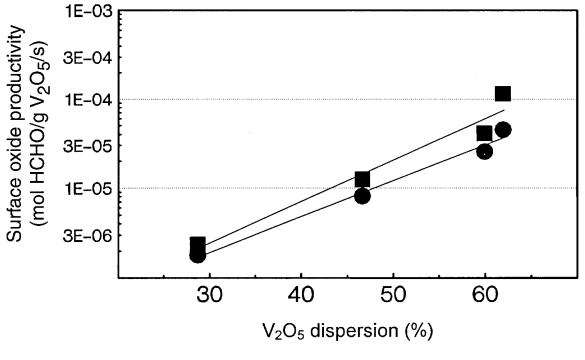

FIG. 9. Relationship between specific oxide productivity at 600°C (●) and 650°C (■) and V_2O_5 dispersion of differently loaded VPS catalysts.

Although H_2-TPR results indicate that MoO_3/SiO_2, system is reducible at $T > 400°C$ (Fig. 1), the CH_4-reduction patterns of MPS catalysts (Fig. 4A) point out a very low reactivity of lattice oxygen ions towards CH_4 at $T < 650°C$ (Fig. 4A). At higher T (>650°C), the steep increase in r^* signals the reduction of MoO_3 promoter, leading to the stabilisation of low (<+3) Mo oxidation states which cause the aforesaid carbon deposition. Thus, the lower activity of MPS catalysts at $T \leq 650°C$ is a consequence of a negative *physical* effect of the promoter on the PS surface (1). At higher T, the capability of MoO_3 to interact with CH_4 (Fig. 4A) enhances the SSA of MPS catalysts to values higher than those of PS (1). On this accounts, the rise of E_{app} with MoO_3 loading (1) reflects the increasing extent of *Mc* species which mainly affect the reactivity of MPS catalysts.

The experimental results shown in Table 5 further display that at any T the rate of CH_4 conversion in the absence of gas-phase oxygen (r_0) proves to be two to three orders of magnitude lower than that in the presence of gas-phase oxygen (r_1). This large difference between r_0 and r_1 (Table 5) suggests that the MPO on silica-based oxide catalysts does not proceed through the classic *redox mechanism* involving lattice oxygen ions (2) but rather via a *surface mechanism* based on the activation of gas-phase oxygen on surface "reduced sites" (7, 8). The marked differences in product selectivity (Table 5) prove the occurrence of different reaction pathways in the absence and presence of gas-phase oxygen (7, 8, 39). Indeed, it can be argued that the redox mechanism yield mainly CO (7, 8, 38) as a consequence of the further oxidation of HCHO (Table 5). On the whole, it can be stated that the *concerted or surface mechanism* works much more effectively than the step-wise (Mars–van Krevelen or redox) reaction path, yielding formaldehyde as main reaction product.

Influence of the Support (TiO_2, SiO_2) on the Redox Properties and Reactivity in MPO of Supported Vanadia Catalysts (VT 2, VPS 2)

The H_2-TPR characterization of TiO_2 support indicates that in the range 400–1000°C mostly the reduction of the surface layers of TiO_2 lattice occurs, the maximum reduction rate probably being related to the consumption of the utmost oxygen layer. The enhanced reducibility of both TiO_2 and VT 2 catalysts compared to PS and VPS 2 systems (Table 3) parallels their higher SSA in MPO (1) according to that already observed for other partial oxidation reactions (2, 31, 32, 37). CH_4-TPR results (Fig. 5) also indicate a much higher reactivity towards CH_4 of TiO_2 and VT 2 catalysts compared to PS carrier and VPS 2 catalyst, respectively. Then, even if the agreement between H_2- and CH_4-TPR data allow to explain the superior SSA of

TiO_2-based catalysts in the MPO (1), such data cannot provide a valid explanation for their poor HCHO selectivity (1). According to the findings of Wachs *et al.* (40) concerning the partial oxidation of *o*-xylene on V_2O_5/TiO_2 catalysts, the marked tendency of TiO_2 based systems to promote the further oxidation of HCHO to CO can be attributed to the high oxidizing strength of "exposed" TiO_2 sites. This is further supported by the product distribution obtained in absence of gas phase oxygen on TiO_2 and VT 2 sampel (Table 6). In fact, the addition of V_2O_5 to TiO_2, besides implying an enhancement in the reactivity, gives rise to the formation of HCHO not observed under the same conditions on the bare TiO_2 support.

CONCLUSIONS

The redox and surface properties of SiO_2, TiO_2, MoO_3/SiO_2, V_2O_5/SiO_2, and V_2O_5/TiO_2 systems, investigated by H_2-TPR, CH_4-TPR, and oxygen chemisorption methods, allow the drawing out of the following structure–activity relationships:

1. The capability of the silica surface to interact with CH_4 forming both methoxy and methyl complexes accounts for its peculiar catalytic pattern in the MPO.

2. The relative concentration of *Im* and *Mc* in MoO_3/SiO_2 and *Iv*, *Pv*, and *Vc* in V_2O_5/SiO_2 catalysts controls their catalytic patterns in MPO:

   a. For low–medium loaded (<10 wt%) catalysts, the different effect of MoO_3 and V_2O_5 promoters on the functionality of the silica support at $T \leq 650^\circ$C is a consequence of the different reducibility pattern of *Im* and *Iv* species, respectively.

   b. The prevailing extent of *Vc* in highly loaded (>10 wt%) V_2O_5/SiO_2 catalysts implies a shift from *surface* to the *redox* reaction mechanism, resulting in a lower effectiveness in terms of both activity and HCHO selectivity.

   c. For medium loaded (7 wt%) MoO_3/SiO_2 catalysts the easier reducibility of *Mc* results in a promoting effect on activity and HCHO productivity of PS carrier at $T > 650^\circ$C.

3. The weaker oxygen bonding in TiO_2 support confers a higher reacitvity to V_2O_5/TiO_2 catalysts with respect to V_2O_5/SiO_2 systems in MPO.

4. The most effective reaction path of MPO on silica based oxide catalysts involves the direct participation of gas-phase oxygen activated on the surface reduced sites.

REFERENCES

1. Parmaliana, A., and Arena, F., *J. Catal.*
2. Sokolovskii, V., *Catal. Rev.-Sci. Eng.* **32**(1 & 2), 1 (1990).
3. Pitchai, R., and Klier, K., *Catal. Rev.-Sci. Eng.* **28**(1), 13 (1986).
4. Brown, M. J., and Parkins, N. D., *Catal. Today* **8**, 305 (1991).
5. Kennedy, M., Sexton, A., Kartheuser, B., Mac Giolla Coda, E., McMonagle, J. B., and Hodnett, B. K., *Catal. Today* **13**, 447 (1992).
6. Koranne, M. M., Goodwin, J. C., and Marcelin, G., *J. Phys. Chem.* **97**, 673 (1993).
7. Parmaliana, A., Sokolovskii, V., Miceli, D., Arena, F., and Giordano, N., *in* "Catalytic Selective Oxidation" (S. T. Oyama and J. W. Hightower, Eds.), ACS Symp.Series 523, p. 43. Washington, DC, 1993.
8. Parmaliana, A., Sokolovskii, V., Miceli, D., Arena, F., and Giordano, N., *J. Catal.* **148**, 514 (1994).
9. Sun, Q., Herman, R. G., and Klier, K., *Catal. Lett.* **16**, 251 (1992).
10. Kartheuser, B., Hodnett, B. K., Zantoff, H., and Baerns, M., *Catal. Lett.* **21**, 209 (1993).
11. Koranne, M. M., Goodwin, J. G., and Marcelin, G., *J. Catal.* **148**, 378 (1994).
12. Mauti, R., and Mims, C.A., *Catal. Lett.* **21**, 201 (1993).
13. Smith, M. R., Zhang, L., Driscoll, S. A., and Ozkan, U. S., *Catal. Lett.* **19**, 1 (1993).
14. Smith, M. R., and Ozkan, U. S., *J. Catal.* **141**, 124 (1993).
15. Bañares, M. A., Rodriguez-Ramos, I., Guerreor-Ruiz, A., and Fierro, J. L. G., *in* "Proceedings 10th International Congress on Catalysis, Budapest 1992" (L. Guczi, F. Solymosi, and P. Tetenyi, Eds.), Akadémiai Kiadó, Budapest, 1993.
16. Weng, T., and Wolf, E. E., *Appl. Catal.* **96**, 383 (1993).
17. Boreskov, G. K., *Kinet. Catal.* **14**(1), 7 (1973).
18. Kartheuser, B., and Hodnett, B. K., *J. Chem. Soc. Chem. Commin.* 1093 (1993).
19. Miceli, D., Arena, F., Parmaliana, A., Scurrell, M. S., and Sokolovskii, V., *Catal. Lett.* **18**, 283 (1993).
20. Spencer, N. D., *J. Catal.* **109**, 187 (1988).
21. Spencer, N. D., and Pereira, C. J., *J. Catal.* **116**, 399 (1989).
22. Arena, F., Frusteri, F., Parmaliana, A., and Giordano, N., *J. Catal.* **143**, 299 (1993).
23. Arena, F., Frusteri, F., Parmaliana, A., and Giordano, N., *Appl. Catal. A General* **125**, 238 (1995).
24. Desikan, L., Huang, L., and Oyama, S. T., *J. Phys. Chem.* **95**, 10050 (1991).
25. Oyama, S. T., Went, G. T., Lewis, K. B., Bell, A. T., and Somorjai, G. A., *J. Phys. Chem.* **93**, 6786 (1989).
26. Cordero, R. L., Gil Lambias, F. J., and López Agudo, A., *Appl. Catal.* **74**, 125 (1991).
27. Ismail, H. M., Zaki, M. I., Bond, G. C., and Shukri, R., *Appl. Catal.* **72**, L1 (1991).
28. Arena, F., and Parmaliana, A., *J. Phys. Chem.* **100** (1996).
29. Williams, C. C., Ekerdt, J. G., Jehng, J.-M., Hardcastle, F. D., Turek, A. M., and Wachs, I. E., *J. Phys. Chem.* **95**, 8781 (1991).
30. Vikulov, K., Martra, G., Coluccia, S., Miceli, D., Arena, F., Parmaliana, A., and Paukshtis, E., *Catal. Lett.* **37**, 235 (1996).
31. Deo, G., and Wachs, I. E., *J. Catal.* **129**, 307 (1991).
32. Owens, L., and Kung, H. H., *J. Catal.* **144**, 202 (1993).
33. Koranne, M. M., Goodwin, J. G., and Marcelin, G., *J. Catal.* **148**, 369 (1994).
34. Morterra, C., and Low, M. J. D., *Ann. N.Y. Acad. Sci.* **220**(4), 133 (1973).
35. Lischke, G., Hanke, W., Jerschkewitz, H.-G., and Öhlmann, G., *J. Catal.* **91**, 54 (1985).
36. Oyama, S. T., *J. Catal.* **128**, 219 (1991).
37. Mamedov, E. A., and Cortés Corberán, V., *Appl. Catal. A General* **127**, 1 (1995).
38. Oyama, S. T., and Somorjai, G. A., *J. Phys. Chem.* **94**, 5022 (1990).
39. Wachs, I. E., Saleh, R. Y., Chan, S. S., and Chersich, C. C., *Appl. Catal.* **15**, 339 (1985).